THE IMPACT OF GLACIOGENIC SEEDING ON SNOWFALL FROM SHALLOW OROGRAPHIC CLOUDS OVER THE MEDICINE BOW MOUNTAINS IN WYOMING

Binod Pokharel and Bart Geerts
Department of Atmospheric Science, University of Wyoming, Laramie, Wyoming

ABSTRACT. The 2013 AgI Seeding Cloud Impact Investigation (ASCII-13) campaign was conducted over the Medicine Bow range in Wyoming to examine the impact of ground-based glaciogenic seeding on winter orographic clouds and precipitation. The campaign was supported by a network of ground-based instruments, including a microwave radiometer, two profiling Ka-band radars, rawinsonde launches, and a disdrometer. The University of Wyoming King Air with profiling Wyoming Cloud Radar (WCR) conducted eight successful flights in ASCII-13. WCR profiles from these flights are combined with those from seven other flights, which followed the same geographically-fixed pattern in 2008-09.

A case study shows that a clear seeding signature is not apparent in individual WCR reflectivity transects downwind of the silver iodide (AgI) generators, and that natural trends in precipitation over short timescales can easily overwhelm any seeding impact. Therefore the ASCII experimental design included control regions, both upwind of the AgI generators and to the side of the estimated AgI nuclei plumes. Frequency-by-altitude displays show slightly higher reflectivity values during seeding near the ground, at least when compared to the control regions. The near-surface precipitation rate trend from the untreated to the treated period in the target region, compared to that in the control region, varies significantly from flight to flight, according to the WCR reflectivity data within the boundary layer. Most of this variation relates to non-homogenous natural trends across the mountain range, and/or to sample unrepresentativeness, esp. for the control region. While WCR reflectivity profiles from flights over the Medicine Bow range do not show a significant increase in near-surface precipitation during seeding (in comparison with upstream trends), similar data from nine separate flights in 2012 over an adjacent range, the Sierra Madre, do.

1. INTRODUCTION

Geerts et al. (2013) reported on the 2012 AgI Seeding Cloud Impact Investigation (ASCII-12) campaign, conducted over the Sierra Madre in southern Wyoming. Another, somewhat smaller campaign was conducted the following winter (ASCII-13, January-March 2013) over an adjacent range, the Medicine Bow mountains. This article provides a brief overview of the ASCII-13 campaign and preliminary results. The focus is on observations made on board the University of Wyoming King Air, the main research platform in ASCII-13. Included in this survey are results from pre-ASCII flights conducted in 2008 and 2009 over the same mountain range, using the same geographically fixed tracks. Both ASCII-12 and ASCII-13 were supported by the National Science Foundation, and both were conducted in the context of the Wyoming Weather Modification Pilot Project (WWMPP), a 7-year randomized dual-mountain cloud seeding experiment (Breed et al. 2014). The WWMPP is a randomized experiment, in which AgI generators are operated over either the Medicine Bow range *or* the Sierra Madre (Fig. 1). Specific criteria related to wind direction, temperature, and liquid water presence have to be satisfied for at least four hours over *both* mountains, for a WWMPP case to be declared. Then one of the two barriers is selected randomly for ground-based seeding. This cross-over design with two adjacent target areas produces paired data, which requires fewer samples for the same statistical significace, just as a paired t-test requires fewer data than a t-test applied to two independent samples (e.g. Gabriel 1999). More details can be found in Breed et al. (2014). The ASCII-13 project piggybacks on the

WWMPP in the sense that it uses 3-8 AgI generators over the upwind slopes of the Medicine Bow Range, as well as snow gauges in target and control regions, and other probes that characterized the environment, the cloud, and the snowfall.

Mountains in the western United States have been the target of ground based glaciogenic seeding experiments for a long time (e.g., Super and Boe 1988; Super and Heimbach 1988; Deshler et al. 1990; Holroyd et al. 1995; Super 1999; Huggins 2007; Geerts et al. 2010). Glaciogenic seeding of mixed-phase clouds formed when air is forced over these mountains offers good prospects for increasing precipitation in an economically-viable manner (WMO 2010). In fact commercial seeding has been conducted over various mountain ranges in the West for nearly half a century. The efficacy of the glaciogenic seeding remains uncertain (Garstang et al. 2005), and the conditions under which seeding has a positive effect on precipitation remain poorly understood. The generally accepted criteria relate to wind direction, temperature, and presence of liquid water in orographic clouds hugging the mountain. The WWMPP has specific criteria related to these three variables, criteria that need to be satisfied over two adjacent mountain ranges.

The ASCII campaign aims to study the microphysical changes resulting from the ground based AgI seeding in orographic clouds, using both novel instruments (Geerts et al. 2010; Geerts et al. 2013; Pokharel et al. 2014) and numerical modelling that resolves cloud processes, turbulent eddies, and nucleation by AgI (Xue et al. 2013a, b; Chu et al. 2014). This study surveys the ASCII-13 experimental design and observations, with a focus on data from an airborne cloud radar.

The experimental design is described in Section 2. The storm environmental conditions for all flights of the Medicine Bow range are summarized in Section 3. A case study is presented in Section 4. Composite changes in radar reflectivity profiles following the start of AgI seeding are described in Section 5. A broader discussion follows in Section 6. The findings are summarized in Section 7.

2. EXPERIMENTAL DESIGN AND INSTRUMENTS

The ASCII-13 campaign was conducted from January to March of 2013 over the Medicine Bow range, a high, rather isolated range in the interior Rocky Mountains. This mountain range was chosen for two reasons. Firstly, this range was the closest one relative to the home airport for the University of Wyoming King Air (UWKA) research aircraft, amongst the three mountain ranges with WWMPP operations, allowing for more flight time over the mountain, and less in ferry. Secondly, seven flights had been conducted over this range in early 2008 and early 2009 in preparation for ASCII (the "pre-ASCII" flights), and airborne cloud radar profiles from these flights suggested an enhancement of radar reflectivity near the surface downwind of the active AgI generators (Geerts et al. 2010). We wanted to revisit the Medicine Bow range to examine reproducibility of previous results, especially since the pre-ASCII sample size was rather small.

The UWKA operated an array of cloud and precipitation probes, a profiling cloud lidar, and a profiling cloud radar (Wang et al. 2012). Geographically fixed tracks were flown in ASCII-13, as in ASCII-12 (Geerts et al. 2013), including a control leg upwind of the AgI generators and downwind target legs (Fig. 1), intended to isolate any seeding impact from natural storm variations upwind. Two flight patterns were flown.

The Type 1 pattern was a ladder with five rungs, one of them upwind of the three AgI generators designed to be in operation ("leg #1"), and four downwind. This pattern was used for six flights in ASCII-13, and for all seven pre-ASCII flights. Given the orientation of the legs, the Type 1 pattern requires a wind direction between westerly and northwesterly. Legs #2 and #3 are located upstream of the Medicine Bow crest, leg #4 is over the crest and leg #5 is located just downstream of the crest. On most flights, all five legs were flown twice with the AgI generators off, a period referred to as NOSEED.

Then the generators were switched on and an along-wind leg was flown, in part to allow the AgI nuclei to disperse and initiate ice particles. Then all five legs were flown twice again, a period referred to as SEED. During one of the 13 flights (18 February 2013), one of the three AgI generators did not function, resulting in just two generators in operation (Table 1).

The Type 2 pattern was flown when all eight AgI generators (Fig. 1) were used, which occurred just twice in ASCII-13. These two IOPs are also cases for the WWMPP; as described in the Introduction. Since the WWMPP evaluation has not yet been completed at this time, the dates and times of these two cases are omitted in Table 1. The Type 2 control leg was moved further west, upwind of the westernmost generator, and a race track was flown downwind of most generators, over the high terrain (Fig. 1). The flight sequence and NOSEED-SEED partitioning are essentially the same as for the Type 1 pattern. Both the NOSEED and SEED periods involve four race track loops (8 legs) over the mountain, and two control leg passes.

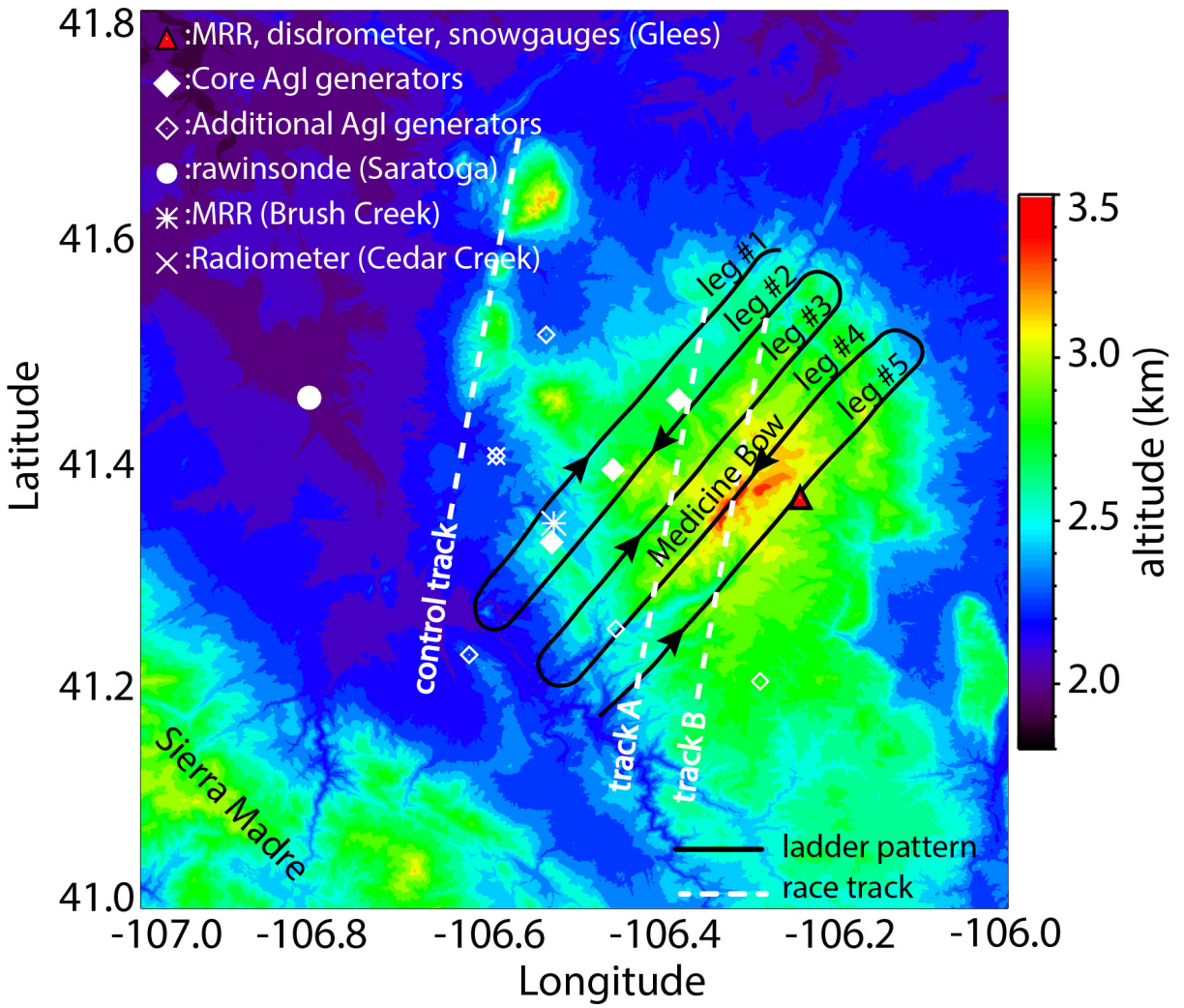


Figure 1: The ASCII-13 experimental design map, showing UWKA flight tracks over the Medicine Bow range. Two types of flight patterns were flown: a) a five-rung ladder pattern (solid lines), used on the 13 flights where only the core AgI generators (filled diamonds) were used; and b) a racetrack and control track (white dashed lines), used on the two flights where the other five generators (hollow diamonds) were used as well. The terrain is shown in the background.

Table 1: Summary of ASCII-13 and pre-ASCII IOPs conducted over Medicine Bow Mountains. The SEED and NOSEED times are based on the UWKA flight tracks. nn is the number of AgI generators in operation during SEED. The different variables given in this table are derived from rawinsonde released from Saratoga, Wyoming (Fig. 1) during the IOPs. The Brunt-Vaisala frequency (N) is the dry (moist) value below (above) the cloud base (LCL). The Froude number (Fr) is calculated as the wind speed divided by N and by the height of Medicine Bow Peak above Saratoga. The wind speed and direction are computed from the average wind vector between the surface and mountain top level. The mean cloud depth is calculated as the vertical distance between the LCL and the WCR echo top (-20 dBZ) height averaged over all legs and ladders. The liquid water path (LWP) is measured by the radiometer at Cedar Creek (Fig. 1).

date	time (UTC)						nn	700 mb T	cloud base (LCL)		average value from surface to mountain top				mean cloud depth	radio-meter mean LWP
	UWKA NOSEED		UWKA SEED		AgI generator				T	altitude	N	Fr	wind speed	wind dir		
	start	end	start	end	start	end	-	°C	°C	m MSL	10^{-2} s^{-1}	-	m s^{-1}	deg	km	mm
******	******	******	******	******	******	******	8	-17.0	-16.7	2781	0.56	1.73	14.5	268	1.34	0.10
16-Jan-13	0009	0300	0210	0338	0128	0229	3	-13.4	-13.1	2764	1.69	0.28	10.0	269	1.47	0.13
29-Jan-13	2159	2324	2405	2536	2315	2516	3	-16.1	-13.7	2598	0.42	0.97	6.4	338	2.29	0.04
******	******	******	******	******	******	******	8	-8.0	-6.0	2785	0.94	1.57	20.2	277	2.41	0.43
13-Feb-13	0150	0402	0404	0523	0315	0515	3	-12.4	-12.2	2972	1.36	0.41	9.6	254	0.63	0.07
18-Feb-13	1556	1755	1800	1925	1713	1913	2	-14.3	-15.2	3071	0.68	1.36	14.4	283	1.54	0.15
1-Mar-13	0039	0207	0246	0411	0156	0407	3	-10.0	-9.8	3008	0.9	1.11	16.0	297	1.51	0.22
1-Mar-13	2010	2210	2217	2343	1959	2357	3	-6.5	-4.0	2859	0.79	1.00	12.9	298	1.88	0.14
11-Feb-08	2003	2123	2133	2249	2128	2328	3	-9.7	-13.2	2723	0.79	1.33	15.8	319	2.69	0.06
25-Feb-08	2029	2146	2220	2337	2155	2355	3	-8.9	-6.6	2759	0.31	2.65	12.6	295	3.07	N/A
18-Feb-09	1644	1813	1834	1952	1812	2012	3	-10.3	-9.1	2743	0.76	1.19	14.0	304	1.96	0.18
20-Feb-09	2154	2308	2332	2403	2320	2520	3	-10.1	-7.2	2452	0.77	1.30	15.6	309	4.10	0.06
10-Mar-09	1421	1453	1537	1749	1454	1654	3	-17.8	-17.4	2855	0.37	3.88	22.0	274	1.24	0.03
25-Mar-09	1613	1644	1725	1928	1643	1843	3	-10.1	-8.8	2835	0.46	1.96	13.7	266	3.26	0.12
30-Mar-09	1723	1755	1836	2013	1752	1952	3	-16.3	-14.1	2609	0.41	1.77	10.9	324	2.50	0.02

This study focuses on data from the Wyoming Cloud Radar (WCR), a 95 GHz (3 mm) profiling Doppler radar, with fixed antennas pointing down (nadir) and up (zenith) from the aircraft. The vertical vantage point and high resolution of the WCR allow reflectivity profiling down to 50 m above the ground in complex terrain. Cloud seeding is expected to increase the concentration of ice crystals, unforunately radar reflectivity is not a measure of ice crystal concentration alone. Rather, it primarily depends on the size of the scatterers. To a first order, mm-wave radar reflectivity (Z) is a good surrogate measure of precipitation rate (S) (Matrosov 2007; Geerts et al. 2010; Pokharel and Vali 2011), although both variables (Z and S) are integral measures of the particle size distribution with different dependences on the moments of that distribution. The mm-wavelength radar signal can be attenuated significantly in conditions of high liquid water content (Vali and Haimov 2001) and heavy snowfall (Matrosov 2007), but fortunately the targeted storms in ASCII were mostly shallow and light precipitation, so we can assume that attenuation is negligible. WCR reflectivity profiles have been used before to examine the impact of ground-based glaciogenic seeding on orographic precipitation (Geerts et al. 2010; Geerts et al. 2013; Pokharel et al. 2014).

Several instruments on the ground were supported by the WWMPP to collect data during ASCII-13: two fixed Ka-band profiling radars (Micro-Rain Radars, or MRRs) were available, one located upwind of most AgI generators at Brush Creek, and one downwind at GLEES (Fig. 1). The GLEES site is the WWMPP target site for the Medicine Bow range, thus it hosted several snow gauges, and also a Parsivel disdrometer. Rawinsondes were released from Saratoga during each flight, and a passive microwave radiometer was located at Cedar Creek (Fig. 1). One of the measurements from this radiometer is liquid water path (LWP), a vertically integrated quantity. The radiometer was pointed at low elevation angle just above the Medicine Bow range, to capture emissions from low orographic clouds (Breed et al. 2014).

3. ATMOSPHERIC CONDITIONS AND CLOUD PROPERTIES OVER THE MEDICINE BOW RANGE

The upstream atmospheric conditions during the eight ASCII-13 and seven pre-ASCII Intensive Observation Period (IOP) were measured by at least one rawinsonde sounding and the microwave radiometer at Cedar Creek. Conditions during each IOP are summarized in Table 1. The SEED start and end times in Table 1 refer to the period of UWKA measurements over the target and control tracks, with the AgI generators on. The preceding NOSEED period is the same, while the generators were off. The along-wind leg and associated ferry sections typically lasted long enough (~30 minutes) for the AgI nuclei to be advected across the target tracks. In some low-wind cases the SEED period was reduced to account for the delayed arrival time of the AgI plume. The advection time is estimated based on the average wind speed and direction between the surface and mountain top level, listed in Table 1.

The 700 mb temperature was rather cold in most cases ($\leq$-8 ^{o}C in all but one case, Table 1) compared to the cases over Sierra Madre in ASCII-12 (Geerts et al. 2013). A cloud base temperature lower than -8 ^{o}C indicates higher chances of AgI activation: AgI activation increases by 2.5 orders of magnitude between -6 and -10 ^{o}C (DeMott 1997). The low-level wind was relatively strong in most cases ($\geq$10 m s^{-1} in all but one case, and $\geq$20 m s^{-1} in two cases, Table 1). The strong winds supported strong, shear-driven boundary layer turbulence. The well-mixed boundary-layer depth ranged between 0.4-1.2 km above ground level (AGL), and averaged at 0.8 km AGL. This was determined from a spectral analysis of WCR vertical velocity variations along the track, at various heights AGL (Geerts et al. 2011). The low-level wind direction was between 270-315° by design, with some marginal departures from this range, which was tolerated because of the relatively long flight tracks. A wind from 309° is normal to the type I flight legs (Fig. 1).

The Brunt-Vaisala frequency N was rather low compared to typical wintertime continental conditions, N=0.7×10^{-2} s^{-1} on average (Table 1). Here N is calculated as an average of the dry N from the near-surface mixed layer to the lifting condensation level (LCL), and as the moist N from the LCL to mountain top level, i.e. it represents the stability of a parcel lifted from the upwind boundary layer to mountain top. In some cases there was some potential instability, i.e. the equivalent potential temperature decreased with height below mountain top level (not shown).

Consistent with the strong wind and low stability, the Froude number of the upwind flow was rather high, $Fr \geq 1$ in almost all cases. This Froude number is calculated using the mean wind (U) and stability (N) listed in Table 1, as $Fr=U/NH$, where H is the height difference between Saratoga and mountain top level. In two cases $Fr<<1$, suggesting that in these cases the AgI plumes were channeled around the mountain, and did not reach the target site at GLEES.

The measured clouds during ASCII-13 were mostly shallow, according to WCR reflectivity profile data and the LCL (Table 1). The average cloud depth (computed from the LCL to the WCR echo top) was only 1.6 km in ASCII-13. The seven pre-ASCII storms were slightly deeper (2.7 km on average), with one outlier that was 4.1 km deep. Liquid water was present in the target clouds in all IOPs, according to data from the Cedar Creek radiometer (Table 1), flight-level probes and/or airborne lidar. In all cases the LCL was at least 600 m below mountain top level, so air parcels lifted from the upwind valley should become saturated upwind of the crest. The mean LCL was 80 m below the mean elevation of the three core AgI generators. In the driest sounding, the LCL was 300 m above these generators. IOPs were started only in the presence of visual cloud over the range and/or measurable radiometer LWP.

4. A CASE STUDY: 18 FEBRUARY 2013

We now illustrate the ASCII-13 observations by means of the IOP in the afternoon of 18 February 2013.

4.1 Flow, cloud, and precipitation structure across the mountain

Along-wind legs were flown during each flight after completion of the NOSEED segment, in part to allow AgI nuclei dispersal, in part also to examine the flow and storm structure across the mountain. The along-wind transect for the 18 February 2013 IOP is shown in Fig. 2. The WCR reflectivity transect reveals that the cloud was less than 2 km deep. Rising air motion (WCR hydrometeor vertical motion larger than ~-1 m s^{-1}, the typical fallspeed of snow) prevails on the windward side, and rapid subsidence over a great depth occurs in the lee (Fig. 2b), pulling down the echo top (Fig. 2a). Boundary-layer turbulence can be seen in the lowest ~0.8 km on the windward side, although the boundary-layer top is not as clear as on the ladder legs #3 and #4 (not shown). Turbulence is much deeper (up the echo top) on the lee side, on account of the deep plunging flow. On the upwind side, near 1732 UTC, a distinct liquid water cloud top can be seen below flight level, as a local maximum in the lidar backscatter power, followed by complete attenuation of the lidar signal, and a low depolarization ratio at cloud top level (Fig. 2c and d). This cloud layer is lifted to flight level, and the *in situ* probes record this cloud LW across the mountain (Fig. 2e). Liquid water is mostly or entirely absent in the turbulent snow clouds in the lee of the mountain: the lidar data indicate gradual extinction of the lidar signal into cloud, and a high depolarization ratio, due to non-spherical ice particles. Ice particle concentration varies from 10-20 L^{-1} according to the Cloud Imaging Probe (CIP). The concentration of larger ice crystals measured by the 2DP probe is less than 5 L^{-1} (Fig. 2f). The highest concentration of ice was measured near the mountain peak.

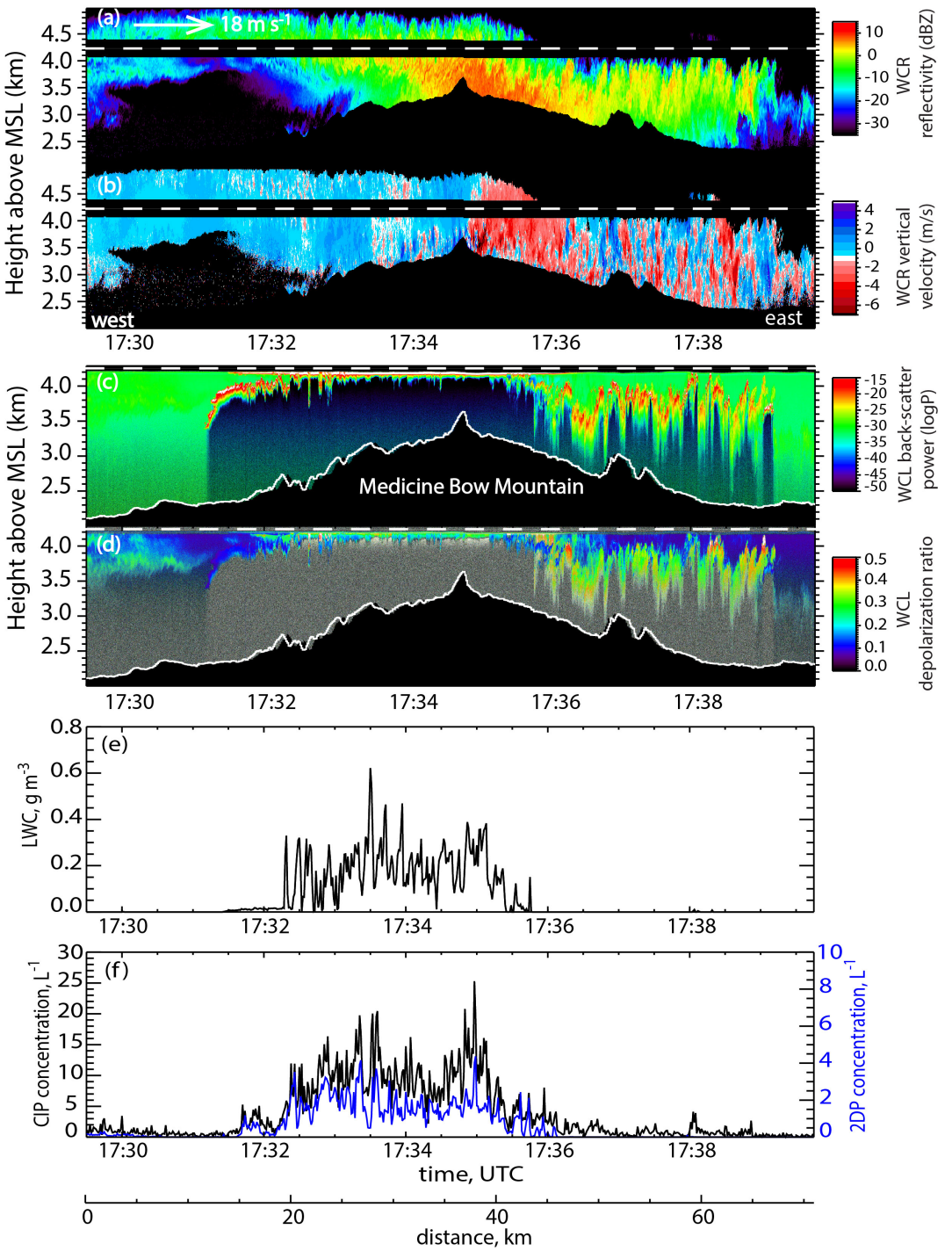


Figure 2: WCR, WCL and in situ probes transect for the along-wind flight leg over the Medicine Bow range on 18 February 2013. The wind direction and UWKA flight is from left (west) to right (east). The flight track was aligned with the low-level wind from 280°. The dashed white line in upper four panels (a-d) is the UWKA flight level. The terrain profile can be seen in these panels. a) WCR radar reflectivity and b) WCR hydrometeor vertical velocity (both above and below the aircraft); c) WCL backscatter power, d) WCL depolarization ratio (both below the aircraft only), e) flight-level liquid water content (LWC) measured by the CDP, and f) flight-level ice concentration measured by the CIP (left y-axis, black line) and 2D-P probes (right y-axis, blue line).

4.2 Upwind atmospheric conditions and suitability for glaciogenic seeding

A deep upper-level trough extended south to southeast of Colorado in the early afternoon of 18 February 2013 with two weak jet streaks: one downstream of the trough over Texas, and one upstream of the trough over western Colorado. A surface low was located in northeast Minnesota with very cold air in the Dakotas. This synoptic pattern brought some moisture in a cold airmass (700 mb temperature -14°C) over the target mountain, resulting in a shallow orographic cloud over the target mountain. Liquid water persisted in this orographic cloud during the IOP (Fig. 3b); the amount was small, but not unusual for this high-elevation continental location (Table 1). The surrounding valleys were mostly cloud-free and without precipitation.

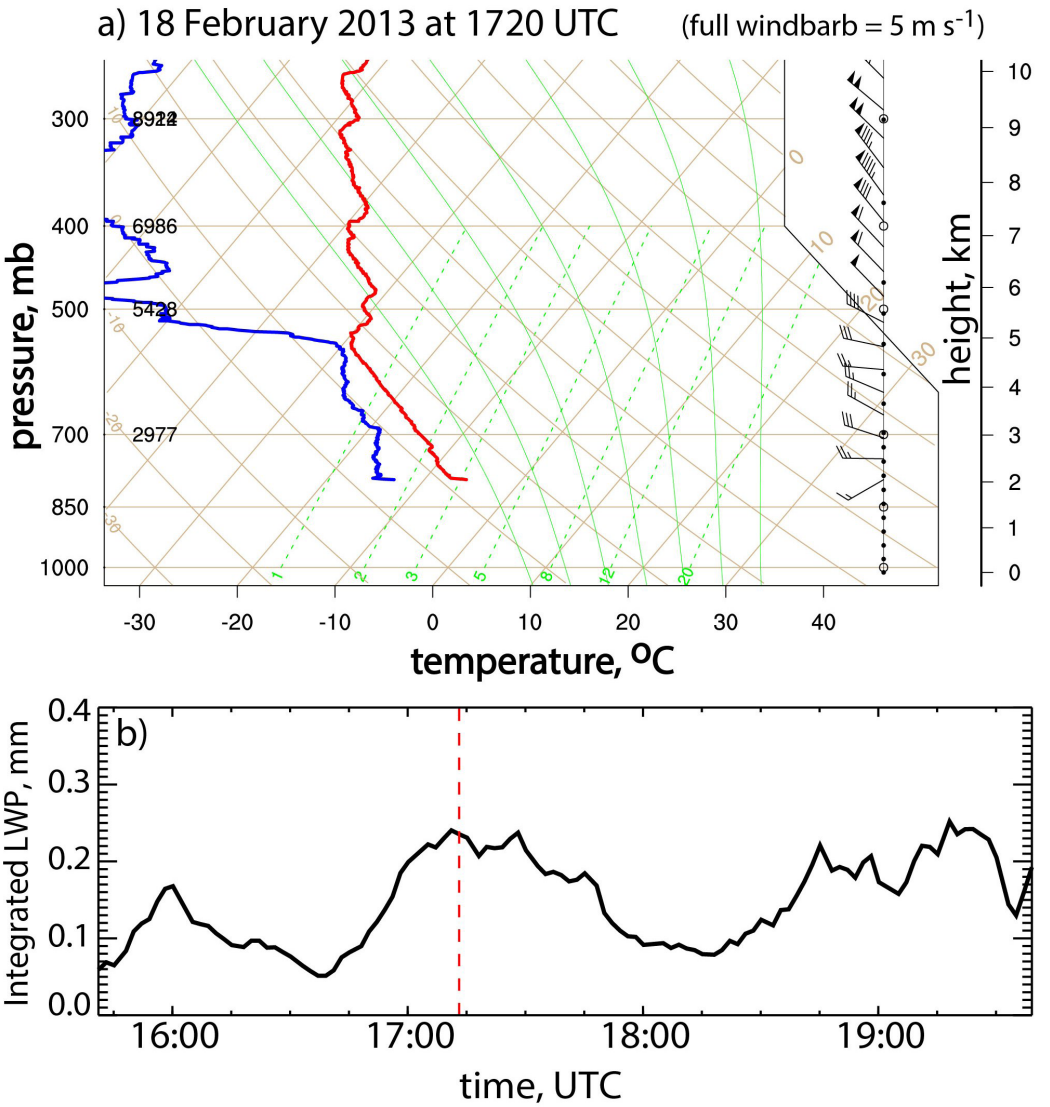


Figure 3: Upstream measurements during the IOP on 18 February 2013. a) Skew T log p display of data from a rawinsonde launched from Saratoga at 1720 UTC and b) liquid water path (LWP) measured by the radiometer located at Cedar Creek (Fig. 1). The vertical dashed line in (b) is the AgI generators activation time.

Surface weather conditions were quite steady according to 5 minutes weather data at Saratoga, GLEES, and Laramie (in the valley just east of the map boundary in Fig. 1). A rawinsonde was launched during the IOP (Fig. 3a). The sounding reveals a rather large lapse rate in the lower troposphere, up to 4.8 km MSL. The wind speed and shear across this lower layer were rather small (Fig. 3a). The near-saturation of air near the top of this layer is consistent with the presence of ice clouds there (see west end of Fig. 2). The Brunt Vaisala frequency *N* from surface to mountain top level would be lower, and convection would be possible, if the boundary layer air had been more humid. The very low humidity results in the highest LCL of all IOPs over this mountain (Table 1). The high LCL implies that the ascending cloud, whose top is seen by lidar in the along-wind leg (Fig. 2c) and in all passes across the upwind ladder legs, likely was less than 1 km deep when it formed upwind of the mountain. Still, the bulk stability *N* was low enough, and the wind speed high enough, to yield a Froude number larger than unity, indicating that the upstream boundary air likely blew over the mountain. This implies that, given a suitable wind direction (283°) a seeding impact is possible along all downstream flight legs, down to leg #5.

In short, the necessary conditions for glaciogenic seeding to impact ice formation and snowfall likely were satisfied, i.e. a low temperature, the presence of cloud liquid water, and a mechanism to lift AgI nuclei into cloud (wind from a good corner). One drawback is that the echo tops were rather cold (-27 to -29°C), cold enough to activate many natural ice nuclei. The thin cloud on the upwind side of the along-wind transect did not have any measurable liquid water (Fig. 2a, e), and could be a source of ice crystals to the lower liquid water cloud lifted over the mountain.

4.3 Cloud radar reflectivity profiles

The UWKA flew over the five geographically fixed legs four times on 18 February 2013, twice before seeding and twice during seeding. The four passages along leg #3, downwind of the AgI generators but upwind of the crest (Fig. 1), are shown in Fig. 4. The along-wind distance between the AgI generators and this leg was ~9 km. This implies ~11 minutes for the AgI nuclei to reach this flight leg, assuming the mean wind listed in Table 1. It is possible that by the time air parcels reach leg #3, the in-cloud residence time of AgI nuclei is not enough for the nuclei to activate and enhance snow growth (e.g., Deshler et al. 1990). Clearly the storm was shallow, less than 2 km deep. Higher level cloud was not observed in these transects. The cloud top was not smooth, but rather, it was marked by "generating cells", small pockets of higher reflectivity, most of them associated with convective turbulence, according to the WCR vertical velocity transects (not shown). This is consistent with the near moist-neutral lapse rate in this layer, according to the sounding (Fig. 3a). These generating cells are present in all 5 legs, mainly legs #3 and #4, and they become stronger and deeper from the first to the last pass.

The projected locations of the two active AgI generators are shown in Fig. 4c and d. There are no well-defined plumes of enhanced mm-wave radar reflectivity downwind of the active AgI generators. The reflectivity is significantly larger than background values in ground-based convective cells downwind of the right-most generator in Fig. 4d. But such convective cells can be seen elsewhere also, e.g. near 19:01 UTC. None of the WCR transects along the target legs on any of 15 flights over the Medicine Bow range show near-surface regions of enhanced reflectivity downwind of each of the active AgI generators. This is a generalization of findings in Geerts et al. (2010) and Chu et al. (2014), studies focused on a subset of these 15 cases. The same applies to the nine flights over the Sierra Madre in ASCII-12 (Geerts et al. 2013; Pokharel et al. 2014). In some cases there are suggestions of enhanced reflectivity plumes where they are expected, but this likely is fortuitous, since not a single transect shows 3 (or 2) plumes downwind of the 3 (or 2) active generators.

This does not mean that AgI seeding did not affect reflectivity in any of these cases. Rather, the diffusion pattern of AgI nuclei and AgI-impacted snow in the windy, turbulent boundary layer over these mountain ranges is quite complex (Xue et al. 2014). Therefore changes in reflectivity have to be examined in a composite sense.

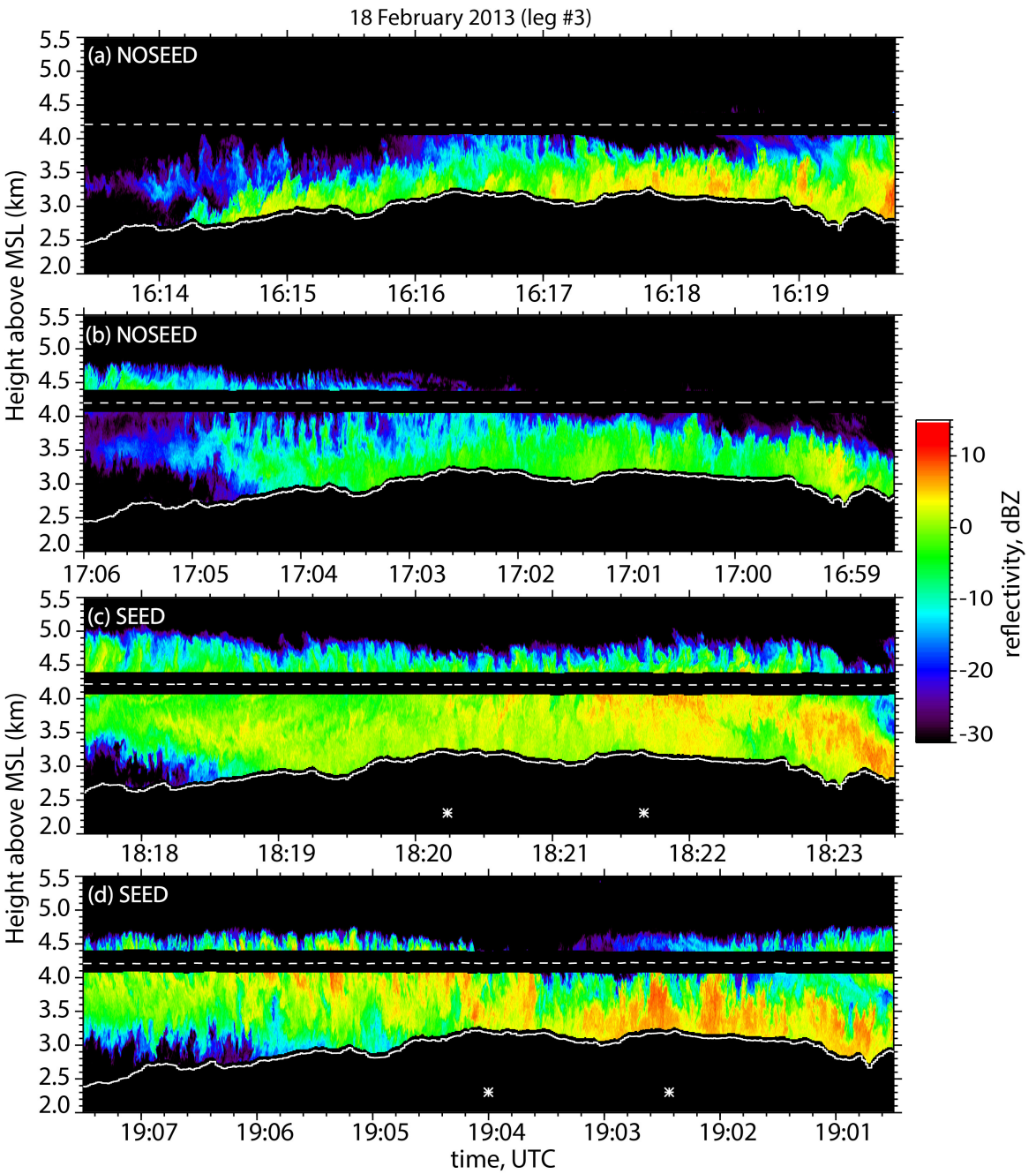


Figure 4: Example UWKA radar reflectivity transects, collected along flight leg #3 (Fig. 1) on 18 February 2013. The transect is oriented from SW (left) to NE (right). The flow is mainly into the page, but the low-level wind has a component from left to right, consistent with the sounding (Fig. 3a). The upper (lower) two panels apply to the NOSEED (SEED) period. The star symbols in the lower two panels show the projection of the two AgI generators active in this IOP.

4.4 Radar reflectivity composites

WCR reflectivity from all 16 passes in the target region (4 ladders, 4 legs) are composited in normalized frequency by altitude diagrams (FADs) in Fig. 5a. The construction of these FADs is explained in Geerts et al. (2010). In essence, WCR pixels are binned as a function of their height AGL (not MSL) and reflectivity value. The FAD confirms the storm's shallow depth: above 1.5 km AGL, less than a third of the profiles have any values (see data presence line in Fig. 5a), and the reflectivity values are close to the sensitivity threshold of a typical weather radar at a typical range of tens of km. Snowflakes grow rapidly towards ground level, and snowfall is widespread near the ground, churned by turbulence. The reflectivity near the ground averages at just 2 dBZ, which corresponds with a light snowfall rate (~0.15 mm h^{-1}).

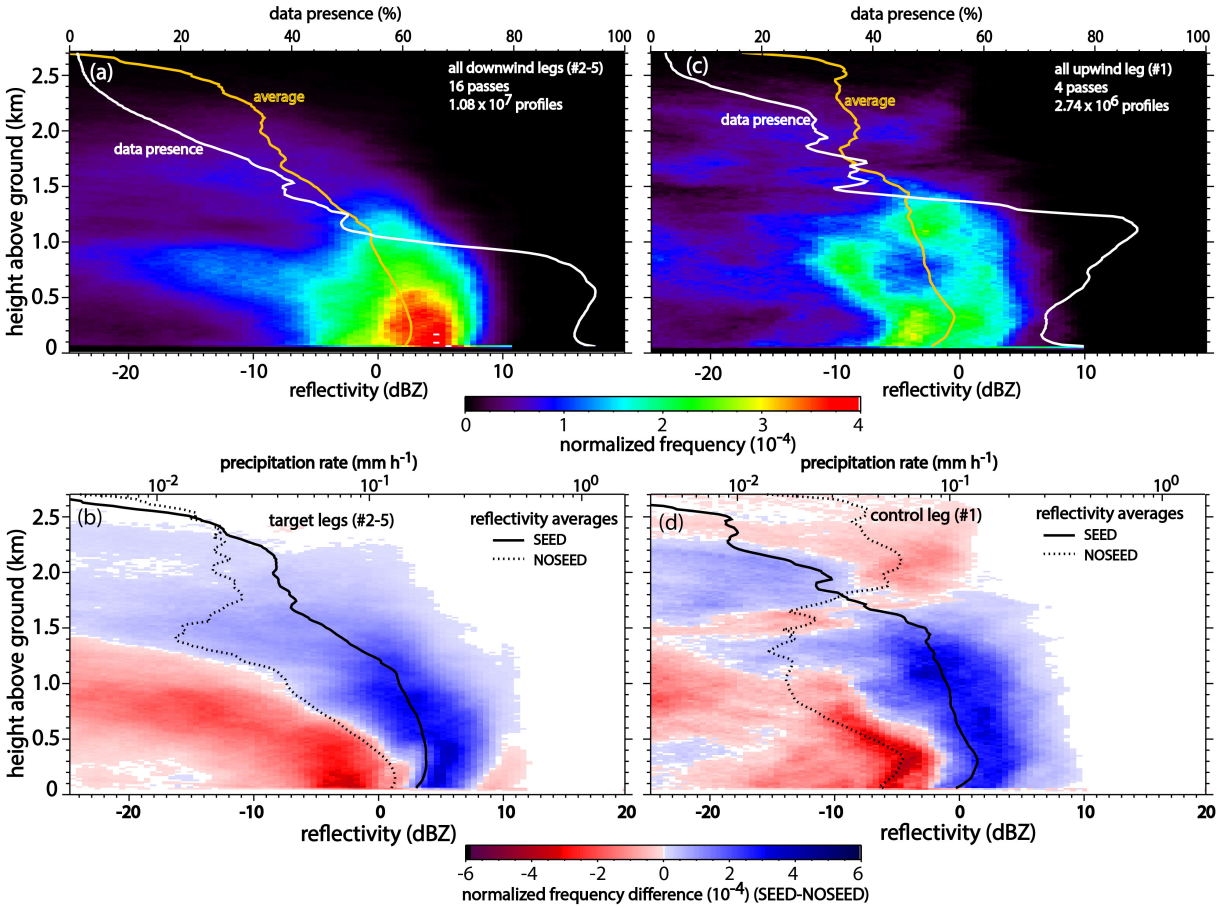


Figure 5: Normalized frequency by altitude diagrams (FAD) of WCR reflectivity (Z) for the flight on 18 February 2013. (a) FAD for all four passes over the target legs (#2-5) during the IOP; (b) difference FAD (SEED minus NOSEED) for the same target legs. The average reflectivity profiles are shown as a yellow line in (a) and as black lines in (b). The "data presence" (white line in (a)) is the fraction of WCR profiles with data in each height bin. The precipitation rate (S) shown in the upper abscissa of (b) is inferred from $S=0.39\ Z^{0.58}$. (c) and (d) correspond with (a) and (b), but apply to the control leg (#1).

Next, the same WCR reflectivity profiles are partitioned in two parts (the first two ladders are NOSEED, the last two ladders are SEED), then composited as before, and since the FAD counts are normalized (the sum of the values in all bins equals 1), bin-by-bin differences can be taken, such that we can compare the relative frequency of a reflectivity value at a certain height AGL during the SEED period to that during the NOSEED period. This is the reflectivity *difference* FAD, shown in Fig. 5b. This clearly shows that the probability of higher reflectivity (heavier snowfall rate) is larger during the SEED period, at all levels. (The sample size above ~1.5 km AGL is very small, thus those differences are not significant.) The increase in storm intensity is evident from Fig. 4 and from the average reflectivity lines in Fig. 5b. This higher reflectivity may be due to AgI seeding, especially if it is concentrated close to the ground, but any trend in the control region needs to be examined first, before drawing any conclusion.

The WCR reflectivity profiles for the four passes over the control leg (leg #1) are composited in the same way (Fig. 5c). The mean near-surface reflectivity is about 3 dBZ higher over the mountain (legs #2-5, Fig. 5a) than over the foothills (leg #1); this is natural orographic enhancement. The corresponding reflectivity difference FAD for leg #1 (Fig. 5d) also shows storm intensification at all levels during the SEED period. In fact the trend is larger for the control leg than for the target legs: the (SEED-NOSEED) difference of the mean reflectivity values in the lowest 0.8 km (the boundary-layer depth) is 6 dBZ for the control leg (Fig. 5d) and 3 dBZ for the target legs (Fig. 5b). If an identical natural trend over control and target areas is assumed, then one must conclude that AgI seeding has no positive impact on reflectivity, and therefore on snowfall rate, during this IOP. It is quite likely that over this short timescale the trends over leg #1 and the adjacent legs #2-5 are not the same. Also, precipitation becomes more convective during ladder 4 as generating cells deepen (Fig. 4), and the control region is just a single leg, where passing cells may be intercepted, or missed. This case study highlights the challenge of isolating the impact of seeding on precipitation in individual case studies. Therefore we summarize changes in the target region (relative to the control region) for all flights over the Medicine Bow range.

5. Composite WCR reflectivity profiles for all flights over the Medicine Bow range

The 18 February 2013 case study demonstrates that natural variability in a storm can readily overwhelm any seeding signature, even for a very sensitive, high-resolution profiling radar. Clearly one case is not sufficient to demonstrate the impact of glaciogenic seeding, and in fact it is not clear from case study analyses alone how many cases would be needed. Here we summarize WCR reflectivity changes for all flights over the Medicine Bow range. Seven flights were conducted during pre-ASCII and eight flights during ASCII-13. The WCR reflectivity profiles collected over the target region (legs #2-5) during ASCII-13 are composited, and the difference (SEED minus NOSEED) FAD is shown in Fig. 6a. This difference FAD can be compared with the corresponding FAD for the seven pre-ASCII flights [Fig. 5c in Geerts et al. (2010)]. The ASCII-13 difference FAD shows that higher reflectivity was more common in the lowest ~1 km during the SEED period in the target region. This is consistent with the seven pre-ASCII flights, which sampled more vigorous storms, on average.

The same difference FAD is computed for the control leg for all ASCII-13 flights (Fig. 6b). Curiously, higher reflectivity was also observed during the SEED period at low levels in the control region. This suggests that storms tended to intensify across the mountain region during these eight flights. While no seeding signature emerges after eight flights (ASCII-13), the combination of the ASCII-13 and pre-ASCII data begins to reveal a (weak) positive seeding impact pattern: high reflectivity values are more common within the boundary layer in the target region during SEED than during NOSEED (Fig. 6c). This analysis involves 12 cases (eight from ASCII-13 and four from pre-ASCII). Only four pre-ASCII cases are included since unfortunately three pre-ASCII

flights were flown without control measurements (just legs #3, 4, and 5). For these 12 cases, the reflectivity difference FAD for the control region does show slightly higher reflectivity during SEED (Fig. 6d), but the pattern is more complex, and lacks a clear low-level dipole structure as in the target region (Fig. 6c). The mean reflectivity trend (SEED minus NOSEED) below 0.8 km AGL (the typical boundary layer depth) in the target region is +2.4 dB, which corresponds a 40% increase of the precipitation rate (S), according to the relationship $S = aZ^b$ (1)

Here reflectivity -Z has units mm^6 m^{-3}, and the water-equivalent precipitation rate S has units mm h^{-1}. The same trend in the control region is just +1.3 dB, or a precipitation rate increase of 20%. We cannot claim either of these differences to be significant.

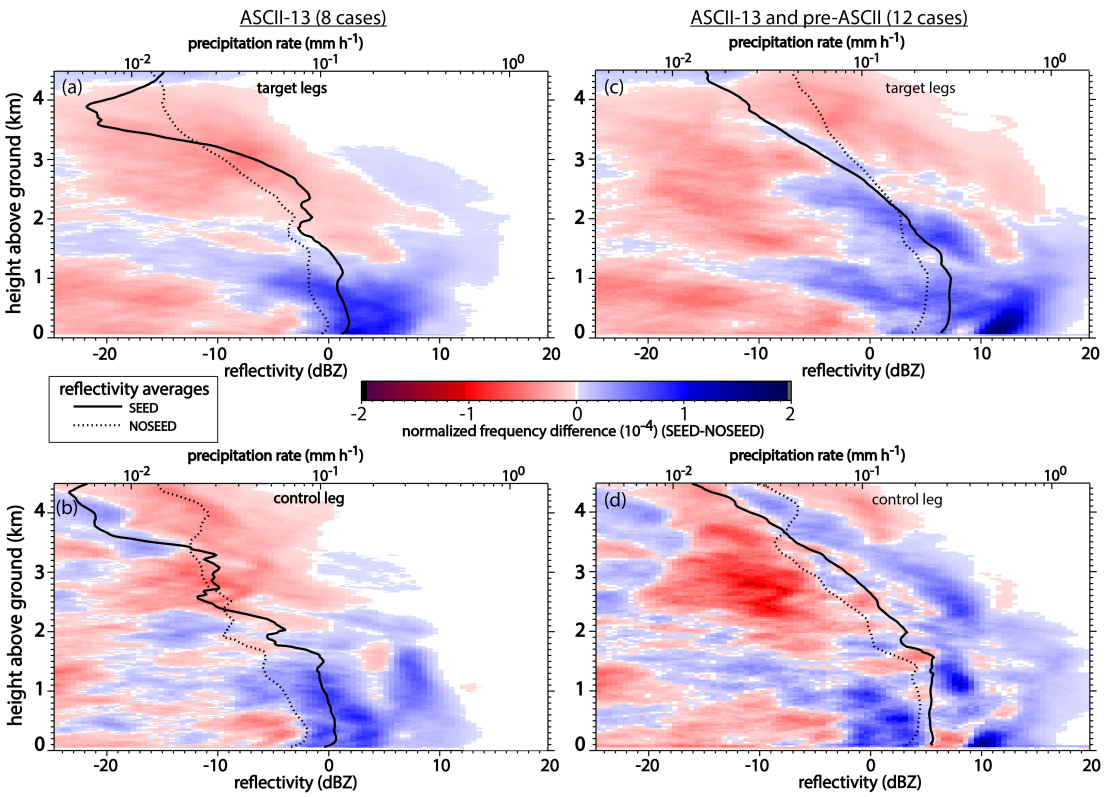


Figure 6: WCR reflectivity difference (SEED minus NOSEED) FADs for eight ASCII-13 flights (left panels) and for eight ASCII-13 plus four pre-ASCII flights (right panels). The target region is shown in the upper panels, the control region in the lower panels.

We use a=0.39, and b=0.58 in equation (1), as in Pokharel and Vali (2011). A different Z-S relationship has been derived for mm-wavelength radar by Matrosov (2007), based on theory. The uncertainty in these relationships is large (larger than factor of two), mainly because of the uncertainty in ice particle density, which is strongly affected by riming. The coefficient a=0.39, and exponent b=0.58 are used here, because they were validated by means of WCR data collected over and near the Medicine Bow range (Pokharel and Vali 2011).

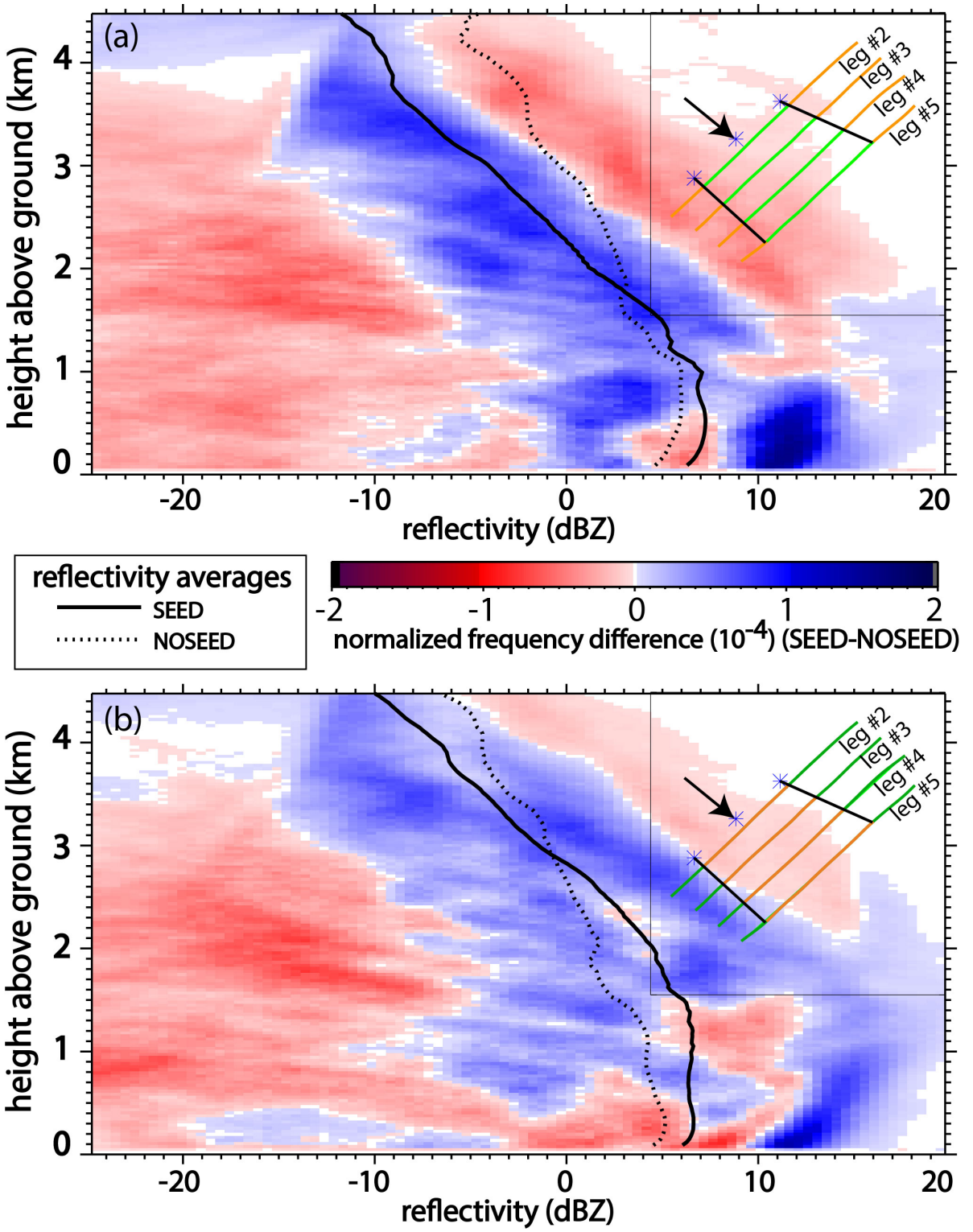


Figure 7: WCR reflectivity difference (SEED minus NOSEED) FADs for target legs (#2-5) of the 13 Type 1 flights a) within the cone shown in the insert schematic map and b) outside this region. WCR profiles are composited for the green flight sections in the insert maps, which also show the location of the three AgI generators. The orientation of the cone varies with the mean wind direction for each IOP (Table 1).

Stronger evidence of a seeding signature emerges when exploring changes in reflectivity in a subsection of the 4 target legs, i.e. a cone downwind of the AgI generators (see schematic insert map in Fig. 7a).

Since there is some evidence that AgI seeding plumes tend to rather narrow, both from observations (Holroyd et al. 1988; Huggins 2007) and from modeling work (Xue et al. 2014), the cone is constructed using the mean wind (Table 1) ±10° from the left- and right-most generators. Only Type 1 flight patterns are used for this (13 flights, core AgI generators only). We examine changes within this cone because ground-based AgI nuclei plumes are most likely to be advected within this cone. The outside sections of the target legs (see schematic insert map in Fig. 7b) then can be considered a "lateral control" region. An advantage of this approach is that the number of target and control WCR profiles is more balanced than the 4:1 ratio for downwind target legs #2-5 and upwind control leg #1.The danger is that especially for low *Fr* cases, the lateral control regions may be impacted by seeding. Higher frequency of enhanced reflectivity is observed in both regions, inside and outside the cone sections, however, the increase in reflectivity is mainly aloft outside the cone, and mainly at lower levels within the cone (Fig. 7). The dipole of increased chances of high reflectivity values and decreased chances of slightly lower reflectivity values within the cone is especially striking (near 6-12 dBZ, in the lowest 0.8 km in Fig. 7a). This suggests a positive impact of ground-based seeding on reflectivity and thus snowfall rate.

6. DISCUSSION

Glaciogenic seeding is hypothesized to increase the number of ice crystals in cloud (e.g., Super and Boe 1988). While probes aboard the UWKA did measure ice particle concentrations and size distributions (e.g., Fig. 2), these data are not used here, because of the low probability of AgI nuclei from ground-based generators to reach flight level in winter orographic clouds. The flight level was 14 kft on most ASCII-13 flight legs, and higher on some. A level of 14 kft corresponds with 610 m above Medicine Bow Peak.

Instead, this study focuses on WCR reflectivity profiles. As mentioned before, a unique advantage of an airborne profiling radar such as the WCR is its ability to measure reflectivity very close to the terrain. A scanning ground-based radar is unable to capture the remarkably shallow snow growth evident in winter orographic storms [e.g., Fig. 4a, and other ASCII studies such as Geerts et al. (2010), Geerts et al. (2013), and Pokharel et al. (2014)], simply because of beam blockage by terrain ridges. Reflectivity profiles near the ground are especially useful for weather modification research, not just because reflectivity changes due to ground-based seeding must be quite shallow, but mainly for the simple reason that the ultimate interest is in precipitation at the surface. Surface snowfall rate is very difficult to measure, especially at short time scales and under strong wind (Rasmussen et al. 2012), and a radar is often the best precipitation gauge (Rasmussen et al. 2003).

It is useful, therefore, to reduce the complexity of the WCR reflectivity FADs to a single number, i.e. the mean reflectivity at low levels, within the turbulent boundary layer. The difference in this number, SEED minus NOSEED, is shown in Fig. 8, for the target region of all 15 flights over the Medicine Bow range. Here the data are averaged below 500 m AGL. The spread in Fig. 8 is quite broad, but some four-fifths of the cases show a positive trend. This does not imply a positive effect of AgI seeding; rather, it simply reflects a trend in snowfall rate during the flights. As shown in the 18 February 2013 case, this trend can be largely natural.

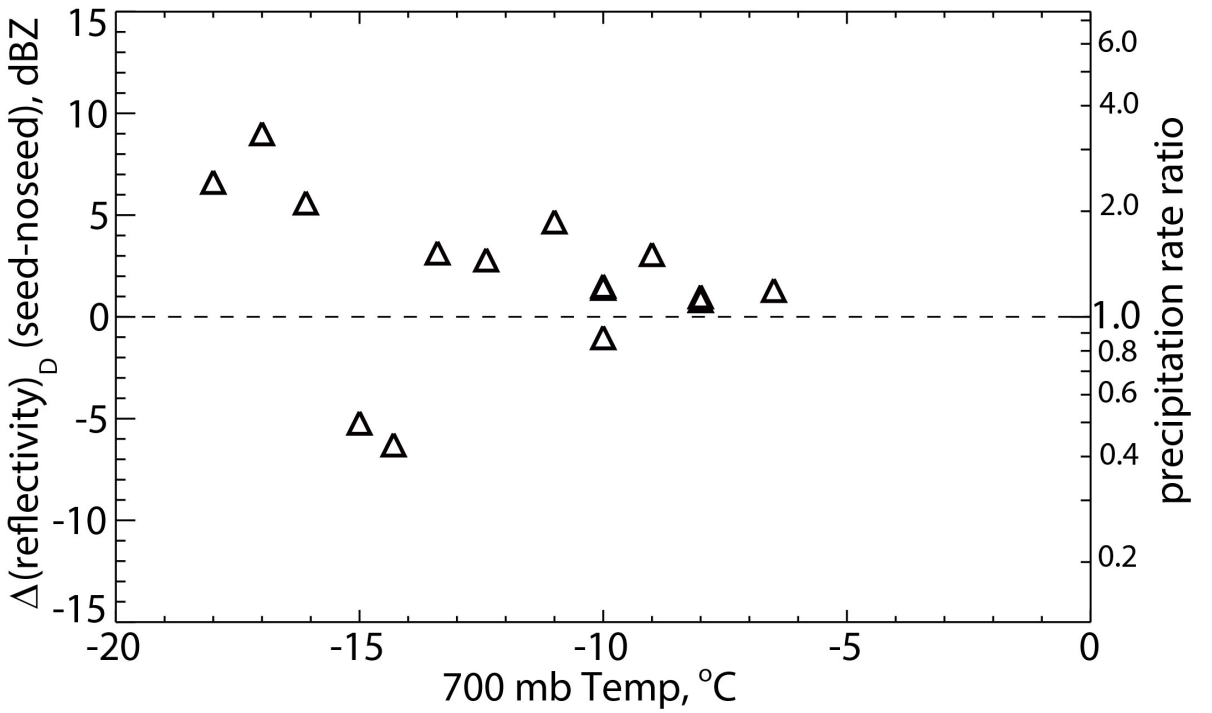


Figure 8: The difference (SEED – NOSEED) in mean WCR reflectivity from target legs below 500 m above the ground according to the 15 flights over the Medicine Bow range. The resulting change in precipitation rate (S) assumes the relation $S=0.39Z^{0.58}$.

One obvious concern could be that the flight periods could have been chosen to be storm intensification periods, based on available forecast guidance. In fact, ASCII IOPs were called for when conditions were suitable according to WWMPP criteria (Breed et al. 2014) over the target mountain, and, as an additional criterion, when conditions were relatively steady, i.e. without frontal passage or significant change in model LWP or precipitation rate during the IOP (Geerts et al. 2013). Maybe the NOSEED-SEED sequence should have been scrambled by design. Given the limited UWKA flight endurance, and the desire to sample the same storm under SEED and NOSEED conditions, seeding had to be conducted during the 2nd half of the flight. Removal of AgI nuclei from the boundary layer after suspension of seeding may take several hours (Heimbach et al. 2008; Super et al. 2010; Xue et al. 2014). This is the reason the WWMPP requires a 4-hour buffer period between cases, to avoid contamination (Breed et al. 2014).

In an attempt to isolate the seeding impact, we compare the trend in the target region (shown in Fig. 8) to that in the control region. Pokharel et al. (2014) devise an expression of reflectivity change in the target area, relative to that in the control area. They define the radar reflectivity impact parameter (ZIP) as the difference between the target average reflectivity change (SEED minus NOSEED) and that in the control region, i.e.

$$ZIP = \Delta dBZ_T - \Delta dBZ_C \qquad (2)$$

where $\Delta dBZ = dBZ_S - dBZ_N$, and subscript S (N) refers to SEED (NOSEED), that is, time periods, while subscript T (C) refers to target (control), that is, locations.

Given that reflectivity Z correlates rather well with precipitation rate S at mm-wave radar frequencies (Geerts et al. 2010), and given our interest in the impact of glaciogenic seeding on S,

we derive another parameter,the precipitation impact factor (PIF), which is defined as a relative change in *S* (SEED compared to NOSEED) in the target area compared to the same relative change in the control area. PIF is calculated as:

$$PIF = \frac{S_{S,T}}{S_{N,T}} \Big/ \frac{S_{S,C}}{S_{N,C}} \qquad (3)$$

Assuming equation (1), PIF is related to ZIP, as follows (Pokharel et al. 2014):

$$PIF = 10^{\frac{(b \times ZIP)}{10}} \qquad (4)$$

A range of values of *b* have been found based on theory (Matrosov 2007) and observations (Geerts et al. 2010; Pokharel and Vali 2011). We assume b = 0.58, as before.

ZIP and PIF values can only be calculated for flights with upstream control measurements. This excludes three pre-ASCII flights. Low level (within 500 m AGL) mean ZIP and PIF values for the remaining 12 flights over the Medicine Bow range and for nine flights over the Sierra Madre (ASCII-12, Geerts et al. 2013) are shown in Fig. 9a. A ZIP value of zero implies the same trend in the target and control areas, i.e. the AgI seeding is neutral. A positive seeding impact is suggested for all but two of the Sierra Madre cases. The verdict is more divided for the Medicine Bow range, with a positive effect on eight flights, a negative effect on three flights, and no effect on the remaining flight. The range of impacts is quite large, especially when expressed in terms of precipitation rate, on average ~40% in either direction. Modelling work suggests much smaller changes in precipitation, in the order of 10% when averaged over a comparably large target area (Chu et al. 2014). This alone is a good indication that the ZIP/PIF values for individual cases are driven not just by seeding, but also by differences in natural trends between control and target regions and/or the non-representativeness of the sampled change in the control region. Because such differences and non-representativeness issues are random, the only way in which confidence can be gained about a true impact of AgI is through the compilation of many cases. Of course there is much value also in detailed process-oriented case studies (e.g., Pokharel et al. 2014) and in modelling studies carefully vetted against observations (e.g., Chu et al. 2014).

The ZIP/PIF values are plotted against 700 mb temperature in Fig. 9. The 700 mb level is about 200 m above the average height of the core AgI generators over the Medicine Bow range, so its temperature is representative of the ambient cloud temperature in regions of AgI-induced ice nucleation. Such nucleation is more likely under *lower* temperatures in the range -17 to -5°C (DeMott 1997). Yet the apparent AgI seeding impact appears more positive under *higher* temperatures in that range (Fig. 9a). This suggests that other factors may affect AgI seeding impact, e.g. fallen snow may be lofted more easily from the surface by wind under lower temperatures. Blowing snow can be a natural source of ice nucleation from the ground (Kristovich et al. 2012).

The average seeding impact over the two mountain ranges is shown in Fig. 9b. Precipitation rate increases by ~20% in the Medicine Bow range and more than doubles in the Sierra Madre. Confidence in these numbers is low, given the wide spread of PIF values in individual cases. A more positive effect over the Sierra Madre may be due to the typically higher temperatures of the ASCII-12 cases (Fig. 9a). (In fact the terrain and the AgI generators are about 300 m lower over the Sierra Madre than the Medicine Bow range, so winter storms typically are warmer over the Sierra Madre.) There may be other factors as well, e.g. related to the terrain shape and the likelihood of blowing snow.

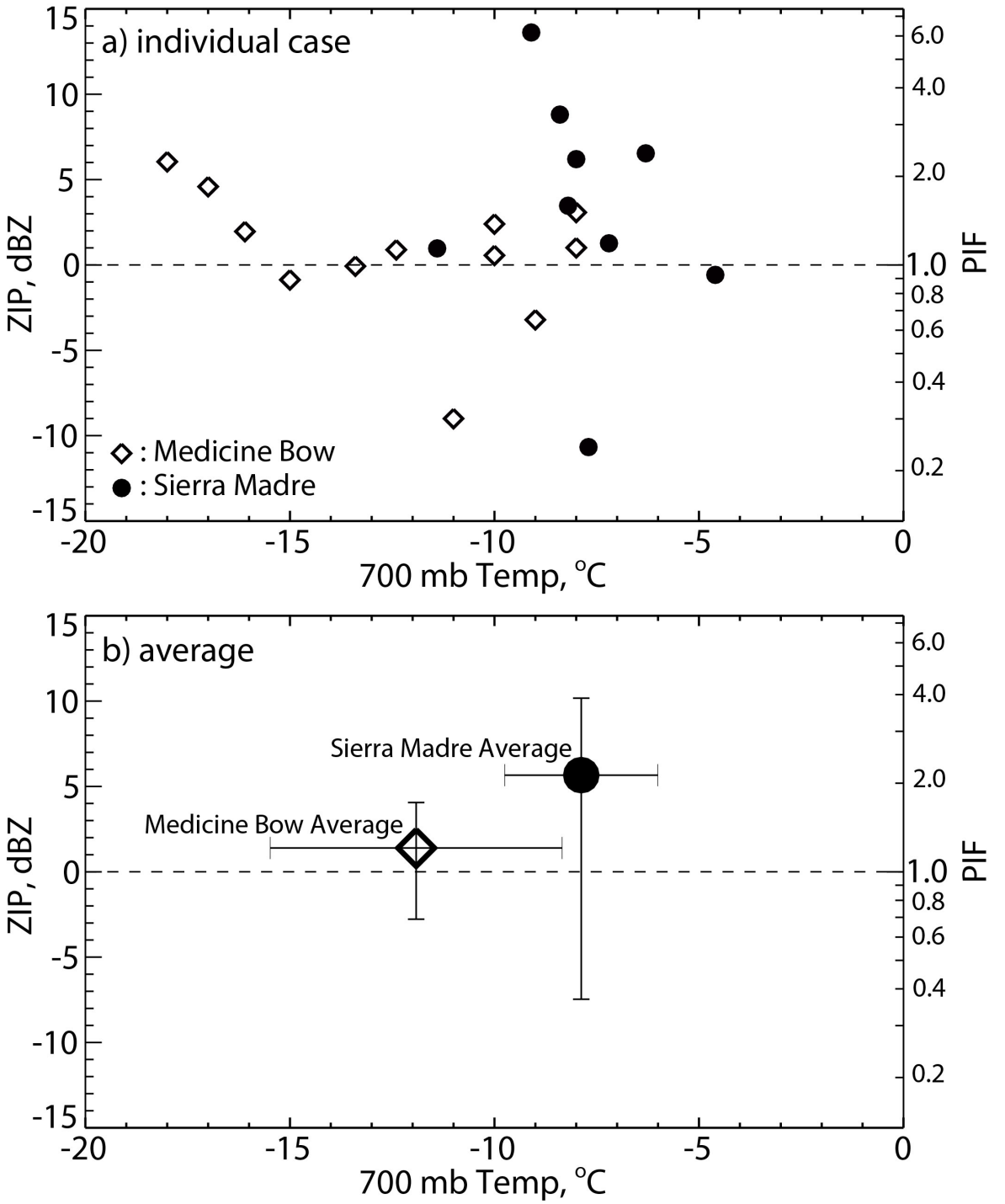


Figure 9: (a) The reflectivity impact parameter (ZIP) and precipitation impact factor (PIF) calculated from the mean WCR reflectivity below 500 m AGL from 21 flights over two mountain ranges (12 flights over the Medicine Bow range and nine flights over the Sierra Madre). (b) As (a), but showing the average value over the two mountains with error bars corresponding to one standard deviation.

7. CONCLUSIONS

The ASCII-13 campaign was conducted over the Medicine Bow range in Wyoming in January-March 2013, to examine how AgI seeding affects orographic clouds and snow growth. Ground-based instruments included a microwave radiometer, two MRRs, and a disdrometer, but not a Doppler-on-Wheels (DOW) radar as in ASCII-12. This study focuses on the profiles of reflectivity from an airborne mm-wave radar, the WCR, which can measure the fine-scale structure of reflectivity down to ~50 m above ground. The following conclusions emerge:

- A case study (18 February 2013) confirms earlier studies that a clear seeding signature is not apparent in reflectivity transects downwind of the AgI generators, and shows that natural trends in precipitation over short timescales readily can overwhelm any seeding impact.
- Therefore it is imperative to estimate this natural trend. In ASCII this was done by flying "upwind control" legs, i.e. upwind of the AgI generators. Also, the target flight legs were long enough that, depending on the wind direction, part of the leg could be considered "lateral control".
- A total of eight shallow storms were sampled in ASCII-13. Exactly the same pattern was flown on seven flights in earlier years. WCR reflectivity FADs collected in the target region downwind of the AgI generators during these 15 flights show that the probability of high reflectivity values close to the ground is higher during seeding, compared to the preceding untreated period.
- This pattern is not present or less evident in a similar difference FAD along the upwind control leg, for a subset of 12 flights for which upwind control legs were flown. It was less pronounced also in the lateral control region for 13 flights with data in that region. Thus, by differencing not just in time (SEED - NOSEED), but also in space (target vs control), a glaciogenic seeding impact signature emerges in the WCR reflectivity for the 12 flights over the Medicine Bow range, although it is weak.
- The near-surface precipitation rate trend from the NOSEED to the SEED period in the target region, compared to that in the control region, varies significantly from case to case, according to the average WCR reflectivity data at low level (within 500 m AGL). Most of this variation relates to non-homogenous natural trends across the mountain range, and/or to unrepresentativeness of the control region.
- Nine flights conducted over an adjacent range, the Sierra Madre, in 2012 reveal a significant positive impact of AgI seeding on low level reflectivity and thus on snowfall rate. It is not cler why the Sierre madre storms were more suitable for glaciogenic seeding than the Medicine Bow storms.

Follow-up work includes cloud-resolving mountain-scale Large Eddy Simulations (100-300 m resolution) of several cases analyzed here. These simulations include a parameterization of ice initiation by AgI nuclei released from a point source (Xue et al., 2013a, b).

ACKNOWLEDGEMENTS

The ASCII campaign is funded by the National Science Foundation grant AGS-1058426. This work also received funding from the Wyoming Water Development Commission and the United States Geological Survey, under the auspices of the University of Wyoming Water Research Program. The operation of the AgI generators, the upstream MRR, and the microwave radiometer was supported by the WWMPP, which is funded by the State of Wyoming and managed by Barry Lawrence. We thank Dan Breed (NCAR) for the Cedar Creek radiometer data, Bruce Boe (WMI) for Saratoga sounding data, Qun Miao for help with the analysis of WCR data, and the UWKA crew, in particular Larry Oolman and Jeff French, for the aircraft operations in ASCII.

REFERENCES

Breed, D., R. Rasmussen, C. Weeks, B. Boe, and T. Deshler, 2014: Evaluating winter orographic cloud seeding: Design of the Wyoming Weather Modification Pilot Project (WWMPP). *J. Appl. Meteor. Climatol.*, **53,** 282-299

Chu, X., L. Xue, B. Geerts, R. Rasmussen, and D. Breed, 2014: A case study of radar observations and WRF LES simulations of the impact of ground-based glaciogenic seeding on orographic clouds and precipitation: Part I: Observations and model validations. *J. Appl. Meteor. Climatol*., doi:10.1175/JAMC-D-14-0017.1, in press.

DeMott, P.J., 1997: Report to North Dakota Atmospheric Resource Board and Weather Modification Incorporated on Tests of the Ice Nucleating Ability of Aerosols Produced by the Lohse Airborne Generator, Dept. Atmos. Sci., Colorado State Univ., Report, Fort Collins, CO, 15 pp.

Deshler, T., D. W. Reynolds, and A.W. Huggins, 1990: Physical response of winter orographic clouds over the Sierra Nevada to airborne seeding using dry ice or silver iodide. *J. Appl. Meteor*., **29**, 288-330.

Gabriel, K. R., 1999: Ratio statistics for randomized experiments in precipitation stimulation. *J. Appl. Meteor*., **38**, 290-301.

Garstang, M., R. Bruintjes, R. Serafin, H. Orville, B. Boe, W. Cotton, and J. Warburton, 2005: Weather modification: Finding common ground. *Bull. Amer. Meteor. Soc*., **86**, 647–655.

Geerts, B., Q. Miao, Y. Yang, R. Rasmussen, and D. Breed, 2010: An airborne profiling radar study of the impact of glaciogenic cloud seeding on snowfall from winter orographic clouds. *J. Atmos. Sci.*, **67**, 3286-3301.

Geerts, B., Q. Miao, and Y. Yang, 2011: Boundary-layer turbulence and orographic precipitation growth in cold clouds: evidence from profiling airborne radar data. *J. Atmos. Sci*., **68**, 2344-2365.

Geerts, B., B. Pokharel, K. Friedrich, D. Breed, R. Rasmussen, Y. Yang, Q. Miao, S. Haimov, B. Boe, and E. Kalina, 2013: The AgI seeding cloud impact investigation (ASCII) campaign 2012: Overview and preliminary results. *J. Weather Mod*., **45**, 24-43.

Heimbach, J. A., Jr., A. B. Super, B. A. Boe, G. Langer, and J. T. McPartland, 2008: Comparison of two acoustic ice nucleus counters. *J. Weather Mod*., **40**, 54-63.

Holroyd, E. W., J. T. McPartland, and A. B. Super, 1988: Observation of silver iodide plumes over the Grand Mesa of Colorado. *J. Appl. Meteor.*, **27**, 1125-1144.

Holroyd, E. W., J. A. Heimbach, and A. B. Super, 1995: Observations and model simulation of AgI seeding within a winter storm over Utah's Wasatch Plateau. *J. Weather Mod*., **27**, 35-56.

Huggins, A. W., 2007: Another wintertime cloud seeding case study with strong evidence of seeding effects. *J. Weather Mod.*, **39**, 9-36.

Kristovich, D. A .R., B. Geerts, Q. Miao, L. Stoecker, and J. M. Ritzman, 2012: Airborne cloud radar and lidar observations of blowing snow during the ASCII project: a possible natural cloud seeding mechanism. AMS 19th Conf. on Mountain Meteorology, Steamboat Springs CO, 20-24 August.

Matrosov, S.Y., 2007: Modeling backscatter properties of snowfall at millimeter wavelengths. *J. Atmos. Sci.*, **64**, 1727–1736.

Pokharel, B., and G. Vali, 2011: Evaluation of collocated measurements of radar reflectivity and particle sizes in ice clouds. *J. Appl. Meteor. Climatol.*, **50**, 2104–2119.

Pokharel, B., B. Geerts, and X. Jing, 2014: The impact of ground-based glaciogenic seeding on orographic clouds and precipitation: a multisensor case study. *J. Appl. Meteor. Climatol.*, **53**, 890-909.

Rasmussen, R., Dixon, M., Vasiloff, S., Hage, F., Knight, S., Vivekanandan, J., Xu, M., 2003. Snow nowcasting using a real-time correlation of radar reflectivity with snow gauge accumulation. *J. Appl. Meteor.*, **42**, 20–36.

Rasmussen, R., B. Baker, J. Kochendorfer, T. Meyers, S. Landolt, A. P. Fischer, J. Black, J. M. Theriault, P. Kucera, D. Gochis, C. Smith, R. Nitu, M. Hall, K. Ikeda, and E. Gutmann, 2012: How well are we measuring snow: The NOAA/FAA/NCAR winter precipitation test bed. *Bull. Amer. Meteor. Soc.*, **93**, 811-829.

Super, A.B., and J.A. Heimbach, 1988: Microphysical effects of wintertime cloud seeding with silver iodide over the Rocky Mountains. Part II: Observations over the Bridger Range, Montana. *J. Appl. Meteor.*, **27**, 1152–1165.

Super, A. B., and B. A. Boe, 1988: Microphysical effects of wintertime cloud seeding with silver iodide over the Rocky Mountains. Part III: Observations over the Grand Mesa, Colorado. *J. Appl. Meteor.*, **27**, 1166-1182.

Super, A. B., 1999: Summary of the NOAA/Utah Atmospheric Modification Program: 1990-1998. *J. Weather Mod.*, **31**, 51-75.

Super, A. B., B. A. Boe, J. A. Heimbach, J. T. McPartland, and G. Langer, 2010: Comparison of silver iodide outputs from two different generators and solutions measured by acoustic ice nucleus counters. *J. Weather Mod*., **42**, 49-60.

Vali, G. and S. Haimov, 2001: Observed extinction by clouds at 95 GHz. *IEEE Trans. Geosc. Rem. Sens*., **39**, 190-193.

Wang, Z., J. French, G. Vali, P. Wechsler, S. Haimov, A. Rodi, M. Deng, D. Leon, J. Snider, L. Peng, and A. L. Pazmany, 2012: Single aircraft integration of remote sensing and in situ sampling for the study of cloud microphysics and dynamics. *Bull. Amer. Meteor. Soc.*, **93**, 653–668.

World Meteorological Organization (WMO), 2010: *Executive summary of the WMO statement on weather modification*. Meeting of the Expert Team on Weather Modification Research, Abu Dhabi, United Arab Emirates, 13 pp.

Xue, L., A. Hashlmoto, M. Murakami, R. Rasmussen, S. Tessendorf, D. Breed, S. Parkinson, P. Holbrook, D. Blestrud, 2013a: AgI cloud seeding effects as seen in WRF simulations. Part I: Model description and idealized 2D sensitivity tests. *J. Appl. Meteor. Climatol*., **52,** 1433-1457.

Xue, L., S. Tessendorf, E. Nelson, R. Rasmussen, D. Breed, S. Parkinson, P. Holbrook, and D. Blestrud, 2013b: AgI cloud seeding effects as seen in WRF simulations. Part II: 3D real case simulations and sensitivity tests. *J. Appl. Meteor. Climatol.*, **52**, 1458-1476.

Xue, L., X. Chu, R. Rasmussen, D. Breed, B. Boe, B. Geerts, 2014: The dispersion of silver iodide particles from ground-based generators over complex terrain. Part 2: WRF Large-Eddy simulations vs. Observations. *J. Appl. Meteor. Climatol*., **53**, 1342-1361.